Original Article

A virtual model of the retina based on histological data as a tool for evaluation of the visual fields

Francisco-Javier Carreras[1], Ángel V. Delgado[2], José L. García-Serrano[3], Javier Medina-Quero[4]

[1]Department of Surgery, Medical School, [2]Department of Applied Physics, School of Sciences, University of Granada, Granada, Spain; [3]Hospital Clínico San Cecilio, University of Granada, Granada, Spain; [4]School of Computer Science, Department of Computer Science and Artificial Intelligence, University of Granada, Granada, Spain

Contributions: (I) Conception and design: FJ Carreras; (II) Administrative support: JL García-Serrano; (III) Provision of study materials and patients: All authors; (IV) Collection and assembly of data: FJ Carreras, J Medina-Quero; (V) Data analysis and interpretation: FJ Carreras, J Medina-Quero; (VI) Manuscript writing: All authors; (VII) Final approval of manuscript: All authors.

Correspondence to: Francisco-Javier Carreras. MD, PhD, Department of Surgery, Medical School, University of Granada, Av. de la Investigación 11, Granada 18016, Spain. Email: fcarrera@ugr.es.

Background: To settle the fundamentals of a numerical procedure that relates retinal ganglion-cell density and threshold sensitivity in the visual field. The sensitivity of a generated retina and visual pathways to virtual stimuli are simulated, and the conditions required to reproduce glaucoma-type defects both in the optic-nerve head (ONH) and visual fields are explored.

Methods: A definition of selected structural elements of the optic pathways is a requisite to a translation of clinical knowledge to computer programs for visual field exploration. The program is able to generate a database of normalized visual fields. The relationship between the number of extant receptive fields and threshold sensitivity is plotted for background sensitivity and corresponding automated perimetry. A solution in two planes to the 3D distribution of axons in the ONH is proposed. Visual fields with induced damage in the optic disc are comparable in pattern and quantity to glaucomatous records.

Results: The two-level simulation of the ONH facilitates the analysis of optic-cup/retinal defects. We can generate the virtual optic pathways tailored to the age and morphology of the patient's eye, and it is possible to reproduce glaucomatous damage by "reverse engineering" engineering. The virtual cortical model renders a quantitative relationship between visual defect and neural damage.

Conclusions: A two-level computing of the retina/optic nerve facilitates the analysis of neuroretinal defects and can be incorporated to automatic perimeters to facilitate visual field analysis.

Keywords: Computer modeling; early optic pathways; neuroretinal defects; threshold sensitivity; visual fields

Received: 12 April 2017; Accepted: 30 April 2017; Published: 23 June 2017.

doi: 10.21037/aes.2017.05.03

View this article at: http://dx.doi.org/10.21037/aes.2017.05.03

Introduction

Only a mere fraction of the available data about visual function form part of a completely understood model (1). Because of diseases that interfere solely with the transmission of the information from the retina to the upper centers of the CNS, it would suffice to simulate the transmission of the most basic visual perception, i.e., contrast sensitivity, to develop a tool that would have clinical significance and applicability. Among visual pathologies, glaucoma stands as a disease that diminishes optic-nerve function in a way that either a channel is functional, or it is not, without intermediate levels of malfunction (2). Glaucoma, in contrast to the fuzzy malfunction of inflammatory or degenerative processes, appears as the reference disease to be modeled, as it represents a consistent source of localized and progressive damage in the anterior optic pathways (3).

As bioanalytical data has little relevance in non-genetic glaucoma, the two main clinical approaches to this disease are the structural (imaging) one and the functional (psychophysical) one. Two main goals in clinical glaucoma are summarized in the questions: does the patient have glaucoma? Is the glaucoma progressing? As no single test can answer these questions, a search for the correct structure/function relationships involves an ever-growing number of both morphological and psychophysical techniques in the clinical arena. The relationship between structure and function has been greatly helped with the introduction of new mathematical and computer models (4-7). Maps that relate structure and function are then refined with comparisons between clinical data, and model output (7-10). Much emphasis is currently being placed on implementing the software used in visual-field testing with mathematical as well as computer simulation to help interpret the results. The set of difficulties in this area of research arise basically from the unreliability of the source of clinical information. Hood *et al.* (11) refer to the "structure-function dissociation" attributing this to several causes, such as normal inter-subject variability, measurement errors, and variable criteria for defining abnormality.

A complementary approach consists of developing a computer-generated model of a segment of the optic pathways with two main guides: first, the principle of retinotopy is strictly adhered to; second, physiological processes that take place, during development, in the formation of the optic stalk, such as the order in which axons enter the optic-nerve head (ONH) (chronotropy), and fasciculation are mimicked (12,13).

Since the initial work of Graham (14) breaking the visual stimulus into parts, a series of computer models reproduce the sensitive response of local arrays in a simulated simplified model of the visual pathways as connected retinal and cortical arrays (15,16). The equivalence between the number of retinal ganglion cells (RGCs) in the retina and the threshold sensitivity can be applied to a modeled retina formed by receptive fields based on empirical data from glaucomatous visual fields. Currently at least four mathematical models, derived from the studies of visual-field variation in glaucoma, relate retinal ganglion-cell number and function (see Malik *et al.* for a review) (17). The visual fields are calculated according to extant *vs.* deleted receptive fields and expressed in linear or logarithmic units (18-21).

The present model deals with the more basic aspects of the structure-function relationship, as the type and number of cells involved in the building of the modeled receptive-perceptive fields, as well as their distribution. Given a density distribution of RGC in the retina, the program autogenerated an ONH, based on the competition for an entry point in the optic stalk, and, as a corollary, the course of axons in the nerve-fiber layer (NFL) (6,7).

Methods

The system represents a number of channels that respond to luminous contrast, formed by three elements: (I) an area in the retina with a variable size related to the precise location; (II) a connecting channel that occupies a specific position in the disc; (III) an area in the cortex with a specific location and a fixed size. Elements a and b give rise to projected visual fields. The cortical representation c is an instrumental step and will be not dealt with here.

Defining the components of the model: RGCs and receptive/perceptive fields

Defining the basic unity of the visual field, the receptive/perceptive field

The dendritic and receptive fields of the RGCs, though approximate, do not exactly match (22-24), but differences are too small to be implemented and our model adheres to a principle of histological coherence. For our purposes the dendritic and receptive fields are morphologically and functionally two equivalent concepts. Resolution thresholds in the central and paracentral retina are linearly related to the separation between RGCs, whereas the relationship is nonlinear beyond 20° eccentricity (25). This discrepancy has been attributed to the finding that proportions of midget and parasol cells at each area of the retina vary with eccentricity (26). The model uses a double mosaic to represent the retina. One mosaic, formed only by midget RGCs subtends light sensitivity (discrimination). The other, which includes not only parasol (which contributes also to sensitivity) but also all other types of RGCs, is used to better represent the actual amount of RGCs eliminated by glaucoma.

Then, when referring to receptive/perceptive fields, we will be dealing exclusively with the sensitive midget mosaic. All receptive fields are considered to have a hexagonal shape, and all hexagons are contiguous (coverage factor one). The hexagons are very small in the center and increase in size towards the periphery. Correspondingly, the density of the receptive fields declines rapidly with

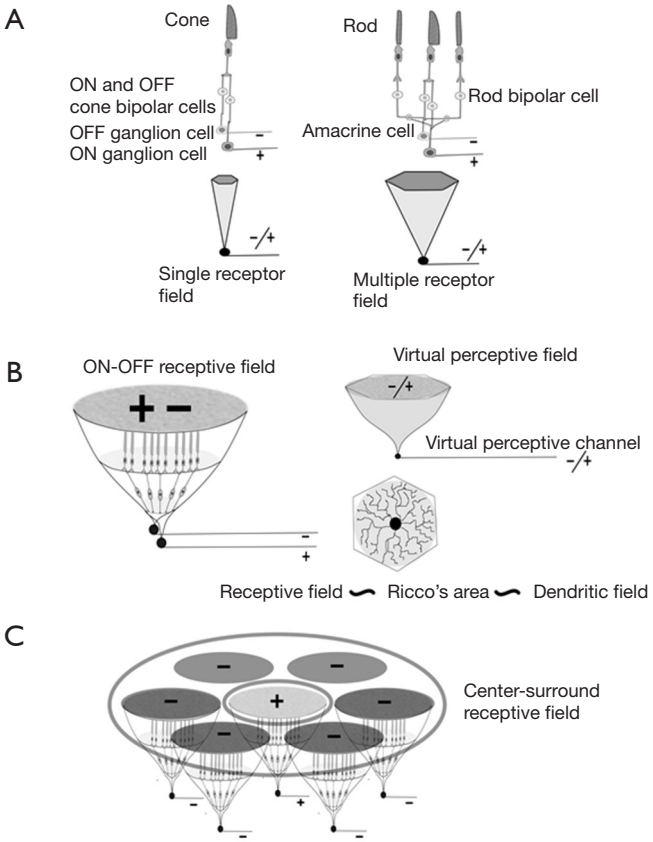

Figure 1 Histological correlates of the basic elements of the simulation. (A) Each single or multiple receptor field is served by two ganglion cells, ON and OFF. The receptive fields can be either unicellular at the foveola or multicellular elsewhere in the retina. Several cone-rod groupings can serve a couple of ON/OFF ganglion cells. The two axons (ON/OFF) are a physiological unit, a perceptive channel; (B) for simulation purposes, the dendritic arbor, the Ricco's area and the receptive field coincide; (C) the physiological response of larger receptive fields with center ON or OFF, and periphery the opposite, is based on the simultaneous activity of the basic units.

distance from the fovea. This is the basis of the limit of the spatial resolution of vision. Although this arrangement may approach the histological relation between soma and dendritic field in peripheral retina, it is certainly not the case within the central 15° of the retina. As a result of a detailed study of the length of Henle fibers (27) a very accurate map of the distribution of the somas of the RGCs was reported. But there is no need to include the actual histological arrangement of RGCs, which is due to a secondary enlargement of cells and displacement of the nuclear area.

Following strictly the histological arrangement of the cellular elements of the retinal transmission chain of the visual impulse, each receptive element (a single-cone receptor if we refer to the fovea) is served by two RGCs, i.e., one ON and one OFF (*Figure 1*). This is the simplest unit and is formed by a single cone, two bipolar cells (ON and OFF) and two RGCs (ON and OFF). The relationship between midget RGCs and the foveal cone has been set at 2:1, but this conclusion has been reached after considerable debate (28). Conflicting estimations vary from 0.9 to 4.0 (27). Part of the problem is due to contamination of the counting with amacrine cells. Finally a ratio of 2.24:1 has been proposed, but then it happens to include bistratified ganglion cells (27). Thus, the only consistent arrangement between cones and midgets is 1:2. Similarly, it can be argued that the coverage factor for magnocellular or parasol cells has been reported as 3 or higher, but this was before Drasdo *et al.* warned about the contamination by amacrines (27); other RGC types can also be misidentified. The coverage factor is incremented because there is a small degree of overlap of neighboring receptive fields, which is considered

desirable for spatial location (29). Any other type of overlap would interfere with discrimination between two points.

When rods participate in the receptive field, visual impulses are transmitted to the cone pathways though the concurrence of an amacrine cell with two connections, one to the ON path and another to the OFF path. Irrespective of the number of rods within a receptive field, the presence of at least one central cone is mandatory for the transmission of a double signal, ON and OFF, to higher centers of the CNS, but an increasing number of cones can be part of the receptive-field arrangement. The same two sets of ON and OFF cells are used by all photoreceptors and are always in line with the cones. The proportion of cones and rods varies with eccentricity.

The complexity of the receptive field structure rises at each successive stage of the visual pathways, higher stages depending on the simpler ones. Basic confluent receptive fields in the retina have a roughly hexagonal shape that matches the dendritic field [1]. After this simple arrangement, the next step in complexity is the center-surround organization, a term coined by Kuffler (30). Center-surround receptive fields imply in our model the confluence of several hexagonal basic ON/OFF fields (*Figure 1*).

Number of retinal receptive/perceptive fields

The retina has probably more than 30 types of RGCs. Although percentages may vary, midget ganglion cells form the most numerous group, up to 70% of all RGCs, while parasol cells account for some 8% to 10%. The retinogeniculate path has only a fraction of the cells, mainly parasol, midget, and bistratified types, which comprise roughly 85% of the optic-nerve axons (1). For the modeling of psychophysical tests, such as the visual field, i.e., dealing with conscious visual pathways, only the ganglion cells linked to the lateral geniculate nucleus (LGN) should be taken into account. Out of all types of RGCs, 12 link to the LGN, but most participate in secondary tasks not related to perception itself. For instance, bistratified ganglion cells, the third most numerous group, relate L/M cones to S cones. In other words, bistratified ganglion cells receive information from the same photoreceptors that also serve midget ganglion cells, and thus this information has been discounted. Very importantly, the same is true of parasol RGCs in relation to midgets. Finally, this consideration can be extended to the other less numerous groups, such as giant-P, epsilon or gamma ganglion cells.

Midget (as well as parasol) RGCs can be divided into two paired groups: ON/OFF. As mentioned above, since the coverage of the midget spans the entire retina, the coverage of the parasol is redundant, and in our model it is only the midget's grid that is used. Then the number of receptive fields must be calculated as 70% of the total number of RGCs, or around 875,000 cells. However, the dendritic fields of the ON and OFF RGCs of each pair are completely fused and occupy identical retinal areas. This is immediately obvious in case of foveal receptive fields in which each individual cone is served by two exclusively dedicated midget ganglion cells (27), and can be safely extended to the organization of increasingly larger receptive fields. This means that the data from the retinal densities of RGCs, must be halved in order to account for the number of ON/OFF receptive fields in the retina. Then the number of ON/OFF channels responsible for contrast perception to be represented in our system is reduced to a number between 400,000 and 500,000 for a standard eye. This reduction is performed maintaining the same local relative density of RGCs as reported by Drasdo *et al.* (27).

Construction of the model

Mosaics of RGCs

Starting from the mosaic (here dubbed 'complete mosaic') just described, based on the data of Drasdo *et al.* (27), we will first generate another complementary matrix based only on the midgets, the cells subjacent to light discrimination, here called "sensitive mosaic".

Complete mosaic

The complete mosaic consists of an improvement over a previous work incorporating refinements (27-32) on the density of midget and parasol ganglion cells, rendering a more accurate map of the retina. Drasdo *et al.* (33) provide accurate estimates of GC displacements from their receptors, improving previous models.

First, the matrix data have been extrapolated from the center to the periphery by means of an ad hoc bilinear interpolation, generating a complete matrix in X range [–90º,60º] and Y range [–60º,60º] based on the 6º×6º interval of the initial data. The starting values of the matrix include the central 24-2 grid of Humphrey's perimetry, with a null value on the external boundary of the retina. The unknown values are calculated by a standard bilinear interpolation applied to trigonometric estimation of 24-2 data in the interpolation box (*Figure 2*).

Once generated, the full-density retina matrix is integrated in the previous random-distribution of RGCs.

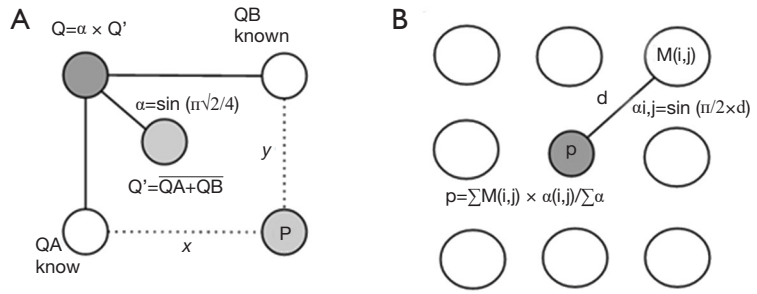

Figure 2 Interpolation process. (A) Extrapolation of the Drasdo values to complete the initial retinal matrix. The cell densities QA and QB are known, and the value in location Q is obtained from the average of QA and QB using the trigonometric distance as weight; (B) interpolation for the calculation of a quasi-continuous density distribution: the density at any point is calculated from the values at neighbor points weighted by their sinusoidal distance to that point.

For this, we have to define a normalized density function [0,1] for each point (x,y) in the continuous ranges X:[–90,60], Y:[–60,60]. To establish this function from the retina density matrix, we applied a nearest-neighbor interpolation process within a window size from the 10º closer matrix data. Due to problems of overshoot, we include a variant that weights the neighbor values based on sinusoidal distance to them (*Figure 2*), generating a smooth distribution function. The standard distribution includes the mean value of 1,200,000 RGCs with ranges from [250,0] RGCs per ratio 0.245º (it is the roundup of the 0.43° of Goldmann III), which agrees with the data from Garway-Heath (34). *Figure 3A* shows the resulting density function for the 1,200,000 RGCs.

Sensitive mosaic

From all cell types that build 20 or so pathways or visual channels (35), we select the mosaic that participates in space discrimination, formed by the midget ganglion cells (*Figure 3B*) calculated from Watson (32). To explore the visual field, we must take into account exclusively the subclasses of RGCs that participate in contrast sensitivity as explored in automated perimetry. However, as the ultimate goal is to identify the structure/function relationship in diseases such as glaucoma and others, then the damaged RGCs need to be considered, and this implies all RGCs.

Modeling light sensitivity across the visual fields requires only the quantitative distribution of midget-cell density as the basis of discrimination, or visual acuity. Functionally, parasol ganglion cells are known to enhance sensitivity. For this reason, the model incorporates their functional activity. In this way, only midget receptive fields are part of the mosaic by the sensitivity incorporating the remaining types of RGCs. It also assumes that the disappearance of a midget implies the disappearance of any other RGC in the immediate vicinity, i.e., midgets represent any other RGC contributing to visual perception present in the retina.

Optic disc/optic nerve

The next step is the generation of the ONH by a procedure that mimics optic-nerve development by fasciculation and orderly growth of the axons. The entry points of each ganglion cell in the optic disk have been selected according to a heuristic location in the retina and a heuristic competition to find the entry point in the nerve. The heuristic parameters define the distance to the fovea and nerve, and the angle to the X axis. Three weights define the relevance of the parameters in the final arrangement.

To find a configuration that could be compared with references in the literature, we applied a local search method to detect proper heuristic-weight values. The new distribution and nerve configuration have improved the results of our previous work, reaching up to 89% similarity (*Figure 4*) with the figures from Jansonius *et al.* (36,37).

A further processing refinement is the generation of a three-dimensional model of the optic disc considering the thickness of the neuro-retinal rim in any sector of the disc. This step allows the projection of localized or scattered neural damage in an area of the disc to the corresponding affected RGCs in the retina and the corresponding visual field (*Figure 4A,B*). We propose to select at least two different planes or coronal sections of the ONH (*Figure 5A,B*). One is the plane already used to determine the position of each axon during the development of the optic stalk. In this plane the distribution of the axons is uniform, without density fluctuations. In the mature optic

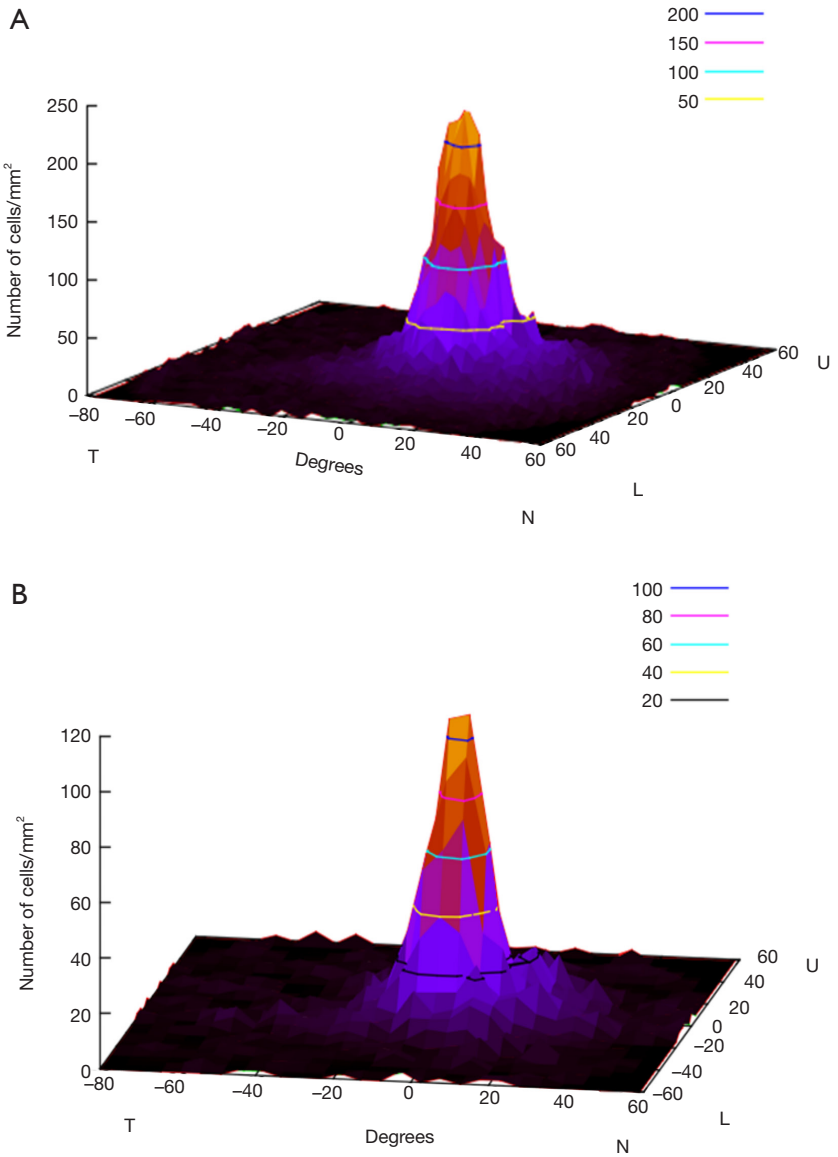

Figure 3 Total RGCs (A) and midget RGCs (B) calculated from Drasdo *et al.* 2007 (27) using bilinear interpolation. T, temporal; N, nasal; L, lower; U, upper retina; RGC, retinal-ganglion cell.

nerve, there is ideally a plane where individual axons, already surrounded by astrocytic expansions, merge in a single bundle before being separated by the columns of astrocytes into singular bundles that pierce the lamina cribrosa sclera (38). This plane is represented in *Figure 5B*, a drawing of a sagittal section of the ONH, by the line of asterisks. The second plane sums up the thicker NFL on top of the preliminar tissue. This layer includes the physiological optic cup and the neuro-retinal rim, with increasing thickness from the center to the periphery of the disc. This plane is represented as a gray square in *Figure 5*. If the optic disc is represented as a perfect circle, then the number of fibers included in a selected wedge is the same, irrespective of the position (rotation) of the wedge. In order to have different numbers of fibers the optic disc should be elliptical or oval. An elliptic disc could project a slightly higher number of fibers per sector in the poles (white sector at 120° in *Figure 5C*). *Figure 6* introduces the central vessels and its protective role on the surface of the optic disc.

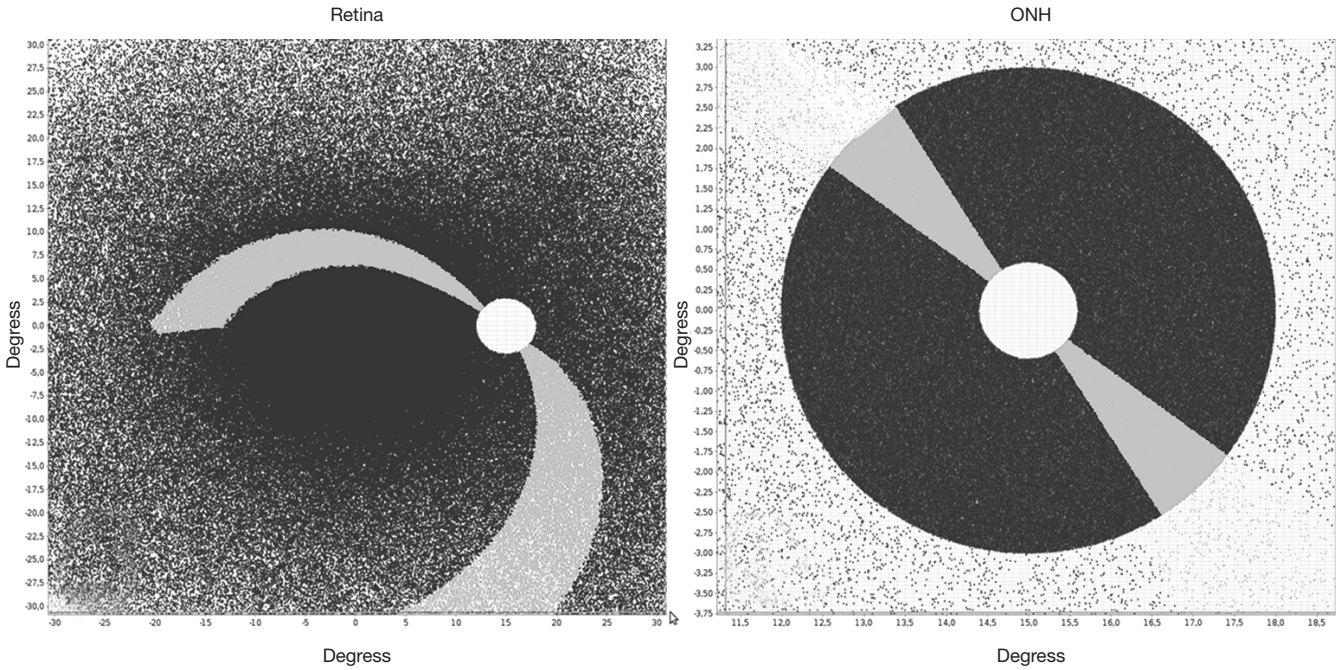

Figure 4 This figure relates the position of a soma (A) in the retina and the entry point in the disc (B). The model reproduces the course of the axons on the retina, which is the base of the Bjerrum scotoma, among other salient features.

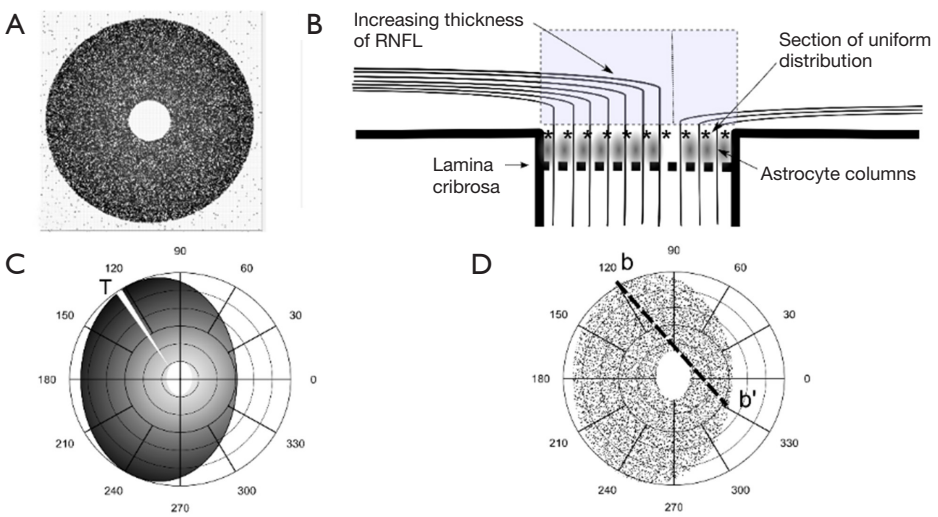

Figure 5 Modeling the neuroretinal rim: frontal plane (X,Y axes) and optic disc section (Z axis). (A) The model initially originates a disc (X,Y axes) of uniform distribution of axons (entry points). This simulates the development of the optic stalk before the vascular invasion, where an almost uniform NFL of regular thickness is formed. In a circular disc the thickness of the NFL is uniform. (B) Z axis. A displacement of the center of the disc in relation to the upper and lower quadrants of the disc would allow for more fibers entering the superior and inferior poles. Consequently, the thickness of the NFL would increase at the poles. The drawing represents a disparity in the number of fibers along the line b-b' of D. (C) The increasing darkness of the gray overtone from the center to the periphery represents the summation of fibers as seen in B. In the poles, the fibers deflected form the overcrowded center are accumulated onto the fibers coming from the adjacent sectors of the retina. (D) Uniform distribution of fibers entry point in an elliptic disc. The b-b' line that dissects the disc in the upper and nasal quadrants, indicates the section of B. NFL, nerve-fiber layer.

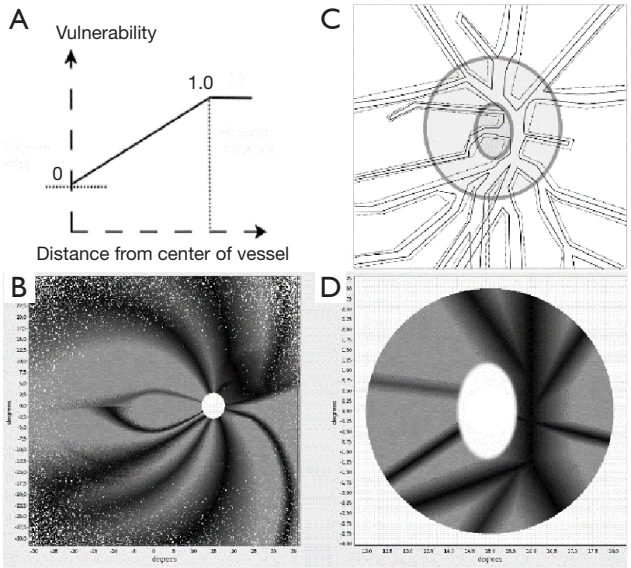

Figure 6 Modeling the neuroretinal rim: setting the vessel on the disc surface. (A) Vascular protection and vulnerability. Probability of radial damage related to the distance to the center of the vessel. The position, size, pattern, and level of protection of the vessel can be adjusted by the user; (B) an example of distribution of the main vessels (solid lines) on the disc surface, along with the perivascular astroglial sheath (dotted lines); (C) projection on the retina of the vascular protective effect at the neuroretinal rim. The protection fades with time as the disease (glaucoma) progresses; (D) distribution of the protection level from the center to the periphery of the vessel.

Visual fields

Contrast sensitivity in normal and damaged pathways

In normal eyes, ganglion-cell density declines with eccentricity. As an advance on our previous model (6), we have built the sensitivity of the retinal mosaic (in terms of probability summation across spatial mechanisms) following a modification to the normal eyes according to the slopes reported by Swanson *et al.* (15), the relation between normal perimetric sensitivity and normal ganglion-cell number had a slope of 1.0 outside 15 degrees and 0.25 within 15 degrees on log/log axes. In glaucomatous eyes, as disease progresses, ganglion-cell density declines, causing the sensitivity of the group of receptive fields to decline correspondingly. Despite the aforementioned differences in slope, we used this same model to predict that, once ganglion-cell loss occurs, sensitivity declines with a slope of 1.0 from this starting value. Swanson *et al.* [2004] (15) explored models of RGC/sensitivity relationships, building retinal mosaics based on real figures of numbers of RGCs and normal retinal sensitivity. When we compared both parameters again in cases of glaucomatous damage, they produced curves relating the remaining RGCs *vs.* sensitivity exploring the responses to several types of pattern stimuli of increasing spatial frequency. Although the use of spatial filters of increased frequency gave curves that showed less sensitivity loss in the initial stages of cell loss and greater sensitivity loss in advanced stages, they concluded that the most probable relationship was linear both in the center and on the periphery. Drasdo *et al.* (33) combined both a linear and a non-linear model to render a set of curves, which proved strikingly similar to those of Swanson *et al.* [2004] (15), and which smoothly combined the linear response on the periphery of the retina with a non-linear response in the central areas.

Based on these recent developments, we used Drasdo *et al.*'s (33) methods of quantifying GC loss in order to build our perimetric sensitivities at each location of a virtual retina and thereby produce the corresponding visual field. As in conventional automated perimetry, we simulated a white circular spot of light, with a diameter of 0.5° (a roundup of the 0.43° of Goldmann III) on a white uniform background. Goldmann III subtends 25.9 min of arc, with an area of 4 mm^2 in the perimeter, corresponding to 0.012 mm^2 on the retina. As we used the size of the Goldmann III stimulus, sensitivity S is expressed as function of the inverse of threshold luminance in decibels, T: $S = 10^{T/T_0}$[1].

Age and contrast-sensitivity threshold

Drasdo *et al.* (33) also proposed a method of age-related change compensation and specified a functional relationship between perimetric sensitivity and GC survival for loss quantification. We used data from the literature to adjust an activation function that fits the empirical data relating the number of RGC to threshold sensitivity and we relate it to the Drasdo's method of age compensation. In this way, we were able to generate a retina for any theoretical subject with a variable population of RGCs (from 700,000 to 1,700,000) and subject the individual to aging, and generate the corresponding average visual field sensitivity at any point in the visual field. Then the standard automated perimetry was performed and the automated visual field was generated. This procedure was applied to quantitative analysis of the effects of ganglion-cell loss in a direct approach by Garway-Heath *et al.* (20) and by Swanson *et al.* (15) in a two-stage model for perimetric sensitivity.

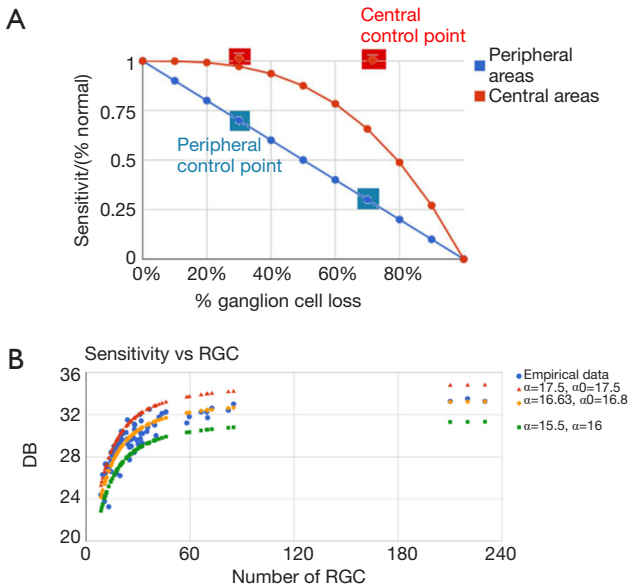

Figure 7 Structure/function relationship in the virtual retina. (A) The graph represents the interval between the sensitivity, expressed as a percentage of the initial value, and extant retinal ganglion cells in central (red) and peripheral (blue) regions of the retina; (B) best adaptation to empirical data and modification of α parameter to higher and lower performances. Relationship between visual-field sensitivity and number of retinal ganglion cells from empirical records (see text). In yellow, an activation function adapts very smoothly to the data with minimum adjustment. A fork between two curves (red and green) is shown to include almost all the empirical data. A chosen curve between those boundaries allows the generation of threshold sensitivities in a sample visual field. Data for graphic (B) at *Figure 7* can be recovered at https://docs.google.com/spreadsheets/d/1f5W2f1rYF94GvT81YzfHPpUUX-j499qDhC0vVVvX9do/edit?usp=sharing.

Projected retinal and visual fields

Retinal fields

With the same mosaic of receptive fields used in the retina we build up a double inverted (right/left and up/down) projection in which the lost receptive fields are marked as erased. As described elsewhere, receptive-field sensitivity is collectively explored as if excited by a Goldmann III stimulus presented in a regular manner to cover the entire visual field. Both mosaics can be explored depending on the aim.

Visual-field estimation

The visual field is estimated in the retina by the density (n) of living ganglion-cells per stimulus area. We propose an activation function which can be suitably adjusted. The main advantage is that it can be adapted to user patterns through three parameters:

(I) α: the saturation value (maximum value of the visual threshold). This would be the sensitivity of the area with the largest density of living cells (i.e., the foveal sensitivity value).

(II) *B*: slope value of the growth curve of the visual field.

(III) Ψ: the minimum number of living cells required to activate the minimal visual field, given by the condition $\log(n)-\psi>0$. Note that the ψ parameter refers to log(n) not to the raw density n.

The expression used for the sensitivity reads:

$$S(n)=\left(1+\frac{1}{1+e^{\beta[\log n-\psi]}}\right)\alpha+\alpha_0 \quad [2]$$

Conventional representation of the visual fields takes into account that each hemi-retina works as a separate unit while the foveal center is split into two halves, both with the value of 0 degrees. As a simplification, despite the temporal field extends up to 110 degrees, the counting stops at 90 degrees.

Results

Simulation of damage by reduction in the number of retino-cortical channels in open angle glaucoma.

The so-called metabolic hypothesis of glaucomatous damage (39,40) defends the antero-posterior progression of axonal damage from the surface to the bottom of the lamina and from the center of the cup to the periphery of the neural rim. Here we reproduce this pattern of damage introducing a protective effect on the fibers under the central vessels. In *Figure 6* we show the areas of the disc protected by the vessels and their projection onto the retinal mosaic.

A stochastic fuzzy method is defined to erode the optic disc on the basis of a percentage of damage. This iterative method accumulates fuzzy random damage both in protected and unprotected areas of the disc, erasing the entry points and the corresponding RGCs. When the fuzzy erosion of a point surpasses the threshold (=1), the entry point is erased. The main characteristic of our approach is that it relates RGC to entry points in nerve in an individual way.

The simulation of damage proceeds by elimination of retino-cortical channels. *Figure 7A* represents the relationship between the sensitivity, expressed as a percentage of the initial value, and extant RGCs in central (red) and peripheral

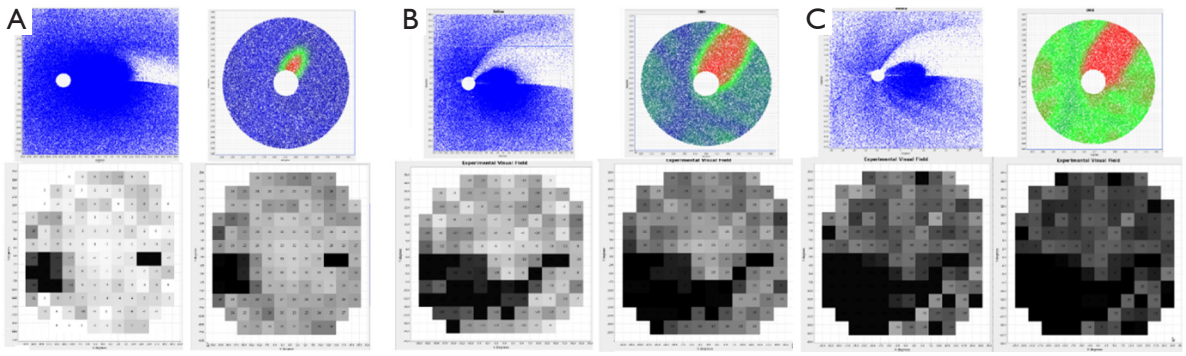

Figure 8 A case example of radial progressive elimination of 20% (A), 50% (B) and 80% (C) of fibers in the ONH and its projection to the affected receptive fields on the retina, with vascular protection activated. All figures labeled I are the representation of the receptive fields. II represents the damaged nerve fibers (red affected, blue not affected). III depicts the corresponding visual field ("Humphrey 32-2") corresponding to the retinal projection of the data in I and II. III shows the reduction in dB in each explored position and IV the remaining sensitivity also in dB. The gray scales are related to the real values, relative or absolute, in dB. These should not be confused with the gray scales in standard automated perimetry, which express the probability of damage in relation to a population of reference.

(blue) regions of the retina.

Under our working hypothesis on the pathogeny of glaucoma, we assume that axons are interrupted at the level of the preliminar region, as a consequence of the astrocyte decay by a form of apoptosis known as anoikis, and caused by calcium withdrawal. The drop in extracellular calcium ion is a consequence of aqueous outflow misdirection (39). The pattern of damage is the initial disappearance of the more superficial fibers, followed by the sequential elimination of the deeper layers. In accordance with the deleterious role of the misplaced aqueous humor, we attribute a protective role to the vessels and their glial sheaths that act as a protective umbrella for the underlying axons (40).

The cortical-pooling model was also used successfully to evaluate the effect of normal aging on sensitivity. *Figure 7B* shows that the parameters α and α0 allow to reproduce the sensitivity data empirically obtained, as well as to predict both higher (younger or healthier subjects) and lower (elderly subjects) performances of the visual field. The agreement found points to the suitability of our model for describing the glaucomatous damage progression.

The program is useful to reproduce any desired pathogenic hypothesis regarding the loss of RGCs fibers. The aim is to use it as a tool to reproduce clinical data, like shape and size of disc and cup, and position and size of central vessels. *Figure 8* depicts a case of glaucomatous progression in three stages corresponding to the elimination of 20%, 50% and 80% of the fibers in the ONH. There we present antero-posterior damage with a protective effect of the central vessels, along with a strong tendency to focalization, i.e., a tendency to deepen the defect rather that to extend it. The shape and size are obtained from an actual photography of the fundus. It is worth noting that the model correctly describes the anisotropic reduction in sensitivity because of the initial distribution of RGCs, reproducing the typical arch form defects of Bjerrum, both in the upper and lower fields with at different stages in the evolution of the defects. Equally interesting is the early appearance of the nasal step, a fact that depends on the correct entry order of RGCs' fibers in the ONH and in the centrifugal expansion of the central excavation. The protective action of vessels can explain the nasal limit (in the retina, temporal in the field) for the progression of the arcuate scotoma. The abundance of remaining central RGCs would account for the persistence of sensitivity in the central area in spite of the early loss of fibers. Final persistence of a temporal island of sensitivity in the visual field is explained by the location of the trunks of the central vessels over the nasal neuroretinal rim.

Discussion

On the RGC/receptive field and RGC/sensitivity relationships

The Swanson-Drasdo model of curves relating RGC loss and retinal sensitivity gives a smooth transition between a linear response on the periphery of the retina and a

non-linear response in central areas. However, in view of the huge discrepancies that this model presents when confronted with data from histological studies on clinical as well as experimental glaucoma, both research teams propose that the differences are attributable to functional loss without a corresponding cellular loss. This indicates that the foundation of the modeling rests on pathological assumptions pertaining to glaucoma. This obligates us to clearly and succinctly state the pathological grounds on which our model is built. Drasdo *et al.* [2008] (33) refer to the shrinkage phase before the onset of apoptosis in the cell (33). This argument is common in the ischemic hypothesis in glaucoma, separating the insult to the cell from the disappearance of the soma. However, it can be pointed out that a delay between the insult and the self-destruction of the soma is common to any model that locates the initial damage to the axons in the ONH or any other point further separated from the soma, and as such does not specifically pertain to the ischemic model. We subscribe to the preliminar location of the initial damage, and we should highlight here that the soma of the RGC may enter apoptosis several weeks after the initial insult to the axons has severed the communication with the brain (2). From this viewpoint, glaucoma is not a slow degenerative disease. If, on the contrary, as aptly expressed by Whitmore *et al.* (2), the neurons function normally until they disappear by a process or compartmentalized destruction, then there should be insufficient time for dysfunction to manifest.

Similar non-linear curves were analyzed by Frisen with a different purpose (41). We would like to point only the inhibitory role of the receptive fields on adjacent fields. This inhibition disappeared with the severing of the axon and could have a positive impact on contrast perception. As a consequence of the lateral inhibition, we can interpret the results of Swanson (15) regarding the relationship between sensitivity (as a percentage of normal) to number of surviving RGCs. The curve in the paracentral field shows better sensitivities than expected. We might think that scattered elimination of ganglion cells could have a positive effect on sensitivity if the lateral inhibition is reduced. It seems counterintuitive that lower spatial frequencies would detect RGC losses more accurately than would high-frequency spatial filters.

On the other side of the analysis rests the animal models of glaucoma in order to relate structure and function. Here the difficulty lies in the animal model itself. Excluding genetic ones, most models known to us are hypertensive (42). They are based on artificially increasing the intraocular pressure in order to induce damage in a relatively short time. There is a notable discrepancy between the empirical data on the number of damaged (or remaining) ganglion cells in moderate and advanced glaucoma either in human subjects or experimental animal models. The difficulty with the animal models of glaucoma is that they may not mimic the real process that takes place in humans. Our critique to models based on the "hypertensive-mechanical-ischemic paradigm" (43), is that they most probably study cases of subacute and progressive ischemia, which is incompatible with the glaucomatous loss suffered over decades in most cases and with moderate or even low levels of pressure (42).

Glaucomatous visual-field pattern and centrifugal progression of the central cup

The site of damage in glaucoma is debated. Classically, glaucomatous damage is considered to be confined to the intraocular portion of the ONH (43). Our model enables the testing of hypothesis about the elimination of fibers in the ONH. Arcuate scotomas are strikingly apparent when the disc vessels are given a protective role. This fact allows the prediction, based on the model, that the initial stages of the progression of arcuate (temporal) and wedge-shaped (nasal) scotomas will have a border or limit demarcated by the position of the vessel in relation to the trajectory of the fibers in the NFL. This prediction could be tested in the clinic in several ways. The model would predict the upper limit of the Bjerrum scotomas, both superior and inferior, based in the position of the temporal branches of the central vessels. Another interesting prediction allowed by the simulation would be to compare the scotomas produced by ischemic defects that would be depending on a capillary defect and consequently unrelated to the position of the central vessels. This enables the simulation as a tool that can be tailored to actual clinical data regarding the morphological data of the disc and the position and relative size of the vessels. The projections of the model can, then, be compared to other clinical explorations as the visual fields and optic disc images (OCT). This would eventually help to interpret quantitatively clinical data from glaucomatous patients.

Damage progression in the z-direction of the neural rim

Spectral domain optical coherence tomography (SDOCT) can provide measurements of the peripapillary retinal nerve fiber layer (RNFL) as well as optic-disc scans. Built-

in software uses a normative database to compare acquired data with RNFL parameters (44). The thickness of the NFL is currently measured at the perimeter of a 3.4 mm diameter disk centered in the optic cup or 2.27 times the optic-disc diameter (1.5 mm average). Alternative measurements are also performed. This produces a RNFL map of the inner region surrounding the optic disc that typically shows a complex double-hump profile with peaks over superonasal and inferonasal sectors (45). Numerous determinants such as age, race, and gender, and axial length heavily influence the results (46). NFL thickness is taken as a proxy measure of the number of axons at each degree of the peripapillary retina. As a result, a projection of the summation of the axons entering a thin wedge of the disc, to the corresponding segment of the periphery of the disc would be a good correlate to the NFL thickness (*Figure 5*). A fiber accumulation appears to happen at the superior and inferior poles of the disc. Apart from number and fiber thickness (parasol being thicker than midget) there are other intrinsic elements that participate in the variability of the NFL thickness around the disc. Variations depend on the presence of vessels and their glial envelope, characterized by its porous nature and the ability to carry fluid (40). The presence of fluid in the preliminar tissue both in the capillary net and in the glial envelope can account for the swift variations in the thickness of the NFL after surgery (47). New measurements are currently being introduced to estimate NFL thickness by the distance between the end of the Bruch membrane and the Elschnig limit that would more strictly correlate with the thickness of the central neuroretinal rim of the central cup (48). This new system has the advantage of avoiding interference by the vessels. The disc distribution of axonal entry points generated by our model is uniform. The generated disc is circular in shape and there is slight decentering of the physiologic cup towards the nasal side. This way of representing the optic nerve does not allows for changes in thickness that the fiber layer shows along the disc periphery, as shown by the clinical measurements of the fiber layer.

The distribution of the axons concentric to the optic cup, which in a later phase is also the site of emergence of the central artery and vein, is the result of the neural fibers entering the optic stalk during the embryonic development of the eye. All this takes place in the absence of vessels. At a later stage the vessels grow into the retina from the remnants of the reabsorbed hyaloid artery. This has importance in the development of our model, as the vessels do not interfere in the course of the fibers, and the thickness of the retinal-fiber layer is thought to be uniform during development, as deduced from the conscriptions of the path-finding mechanisms that give rise to the two main features of timing and fasciculation. The formation of the retinal NFL during development long precedes the vascular invasion. Nerve fibers from RGCs grow towards the optic stalk when the embryonic cleft is in the process of closing at the 15-mm stage (around 31 post-fertilization days). The whole stalk is occupied at 25 mm (around 53 post-fertilization days). However, retinal vascularization starts early in the fourth month (five to six weeks later), emerging from the base of the hyaloid artery, and spreads to the periphery of the retina over the course of four months, reaching completeness only after birth (49).

The order of entry into the optic nerve has been resolved by means of an elliptical pattern of variable flatness. That this situation in part simulates the process taking place during development is testified in the high index of concordance with clinical data (7). We try to find a growth pattern that originates an elliptical disc and provides a better correlation with the data of Jansonius *et al.* [2012] (37). Our present degree of adjustment is close to 90%, the remaining 10% could be due to a polar increase in the NFL. Projection of the number of entry points per sector in an elliptic papilla, as a proxy for the thickness of the peripapillary NFL (*Figure 5*) would render a shallow double-hump configuration.

Conclusions

(I) The model is representative of the relevant components of the visual pathways to retinal and optic nerve diseases such as glaucoma and others (and therefore produces glaucoma-like VF defects when the ONH structures are damaged as in glaucoma, as an example).

(II) Several ways of representing the retina and ONH, incorporating different functional and structural features of optic pathways, are necessary as initial steps towards a more integrated three-dimensional model. With the present model, we propose two mosaics of the retina—one formed exclusively with midget RGCs and other with the complete set of RGCs—together with several sections (coronal and sagittal) of the ONH. The three-dimensional rendering of the optic nerve enables us to deal better with atrophic defects of the preliminar tissue and helps us understand the

effect of the vascular structures in the disc on the pathogenesis of glaucoma.

Acknowledgments

Funding: This research was supported by a grant from the CEI BioTic at the University of Granada, Spain.

Footnote

Conflicts of Interest: The authors have completed the ICMJE uniform disclosure form (available at http://dx.doi.org/10.21037/aes.2017.05.03). The authors have no conflicts of interest to declare.

Ethical Statement: The authors are accountable for all aspects of the work in ensuring that questions related to the accuracy or integrity of any part of the work are appropriately investigated and resolved.

References

1. Rodieck RW. The first steps in seeing. Sunderland, Mass: Sinauer Associates, 1998.
2. Whitmore AV, Libby RT, John SW. Glaucoma: thinking in new ways-a rôle for autonomous axonal self-destruction and other compartmentalised processes? Prog Retin Eye Res 2005;24:639-62.
3. Neufeld AH. New conceptual approaches for pharmacological neuroprotection in glaucomatous neuronal degeneration. J Glaucoma 1998;7:434-8.
4. Denniss J, Mckendrick AM, Turpin A. An anatomically customizable computational model relating the visual field to the optic nerve head in individual eyes. Invest Ophthalmol Vis Sci 2012;53:6981-90.
5. Denniss J, McKendrick AM, Turpin A. Towards Patient-Tailored Perimetry: Automated Perimetry Can Be Improved by Seeding Procedures With Patient-Specific Structural Information. Transl Vis Sci Technol 2013;2:3.
6. Carreras FJ, Rica R, Delgado AV. Modeling the patterns of visual field loss in glaucoma. Optom Vis Sci 2011;88:E63-79.
7. Carreras FJ, Medina J, Ruiz-Lozano M, et al. Virtual tissue engineering and optic pathways: plotting the course of the axons in the retinal nerve fiber layer. Invest Ophthalmol Vis Sci 2014;55:3107-19.
8. Denniss J, Turpin A, Tanabe F, et al. Structure-function mapping: variability and conviction in tracing retinal nerve fiber bundles and comparison to a computational model. Invest Ophthalmol Vis Sci 2014;55:728-36.
9. Erler NS, Bryan SR, Eilers PH, et al. Optimizing structure-function relationship by maximizing correspondence between glaucomatous visual fields and mathematical retinal nerve fiber models. Invest Ophthalmol Vis Sci 2014;55:2350-7.
10. Sugita M, Pircher M, Zotter S, et al. Retinal nerve fiber bundle tracing and analysis in human eye by polarization sensitive OCT. Biomed Opt Express 2015;6:1030-54.
11. Hood DC, Anderson SC, Wall M, et al. A test of a linear model of glaucomatous structure-function loss reveals sources of variability in retinal nerve fiber and visual field measurements. Invest Ophthalmol Vis Sci 2009;50:4254-66.
12. Bunt SM, Horder TJ, Martin KA. The nature of the nerve fibre guidance mechanism responsible for the formation of an orderly central visual projection. Developmental Neurobiology of Vision 1979;27:331-43.
13. Reese BE. Development of the retina and optic pathway. Vision Res 2011;51:613-32.
14. Graham N. Visual pattern analyzers. New York: Oxford University Press, 1989.
15. Swanson WH, Felius J, Pan F. Perimetric defects and ganglion cell damage: interpreting linear relations using a two-stage neural model. Invest Ophthalmol Vis Sci 2004;45:466-72.
16. Gardiner SK, Swanson WH, Demirel S, et al. A two-stage neural spiking model of visual contrast detection in perimetry. Vision Res 2008;48:1859-69.
17. Malik R, Swanson WH, Garway-Heath DF. 'Structure-function relationship' in glaucoma: past thinking and current concepts. Clin Exp Ophthalmol 2012;40:369-80.
18. Robson JG, Graham N. Probability summation and regional variation in contrast sensitivity across the visual field. Vision Res 1981;21:409-18.
19. Redmond T, Garway-Heath DF, Zlatkova MB, et al.

Sensitivity loss in early glaucoma can be mapped to an enlargement of the area of complete spatial summation. Invest Ophthalmol Vis Sci 2010;51:6540-8.
20. Garway-Heath DF, Holder GE, Fitzke FW, et al. Relationship between electrophysiological, psychophysical, and anatomical measurements in glaucoma. Invest Ophthalmol Vis Sci 2002;43:2213-20.
21. Swanson WH, Sun H, Lee BB, et al. Responses of Primate retinal ganglion cells to perimetric stimuli. Invest Ophthalmol Vis Sci 2011;52:764-71.
22. Spillmann L, Ransom-Hogg A, Oehler R. A comparison of perceptive and receptive fields in man and monkey. Hum Neurobiol 1987;6:51-62.
23. Vassilev A, Ivanov I, Zlatkova MB, et al. Human S-cone vision: relationship between perceptive field and ganglion cell dendritic field. J Vis 2005;5:823-33.
24. Peichl L, Wässle H. The structural correlate of the receptive field centre of alpha ganglion cells in the cat retina. J Physiol 1983;341:309-24.
25. Frisén L. High-pass resolution perimetry: central-field neuroretinal correlates. Vision Res 1995;35:293-301.
26. Dacey DM. The Mosaic of midget ganglion cells in the human retina. J Neurosci 1993;13:5334-55.
27. Drasdo N, Millican CL, Katholi CR, et al. The length of Henle fibers in the human retina and a model of ganglion receptive field density in the visual field. Vision Res 2007;47:2901-11.
28. Wässle H, Grünert U, Röhrenbeck J, et al. Retinal ganglion cell density and cortical magnification factor in the Primate. Vision Res 1990;30:1897-911.
29. Lee BB. Receptive field structure in the Primate retina. Vision Res 1996;36:631-44.
30. Kuffler SW. Discharge patterns and functional organization of mammalian retina. J Neurophysiol 1953;16:37-68.
31. Gauthier JL, Field GD, Sher A, et al. Uniform signal redundancy of parasol and midget ganglion cells in Primate retina. J Neurosci 2009;29:4675-80.
32. Watson AB. A formula for human retinal ganglion cell receptive field density as a function of visual field location. J Vis 2014;14(7). pii: 15.
33. Drasdo N, Mortlock KE, North RV. Ganglion cell loss and dysfunction: relationship to perimetric sensitivity. Optom Vis Sci 2008;85:1036-42.
34. Garway-Heath DF, Poinoosawmy D, Fitzke FW, et al. Mapping the visual field to the optic disc in normal tension glaucoma eyes. Ophthalmology 2000;107:1809-15.
35. Dacey DM. Origins of Perception: Retinal Ganglion Cell Diversity and the Creation of Parallel Visual Pathways. In: Gazzaniga MS. editor. The Cognitive Neurosciences. Cambridge/London: The Mit Press, 2004;281.
36. Jansonius NM, Nevalainen J, Selig B, et al. A mathematical description of nerve fiber bundle trajectories and their variability in the human retina. Vision Res 2009;49:2157-63.
37. Jansonius NM, Schiefer J, Nevalainen J, et al. A mathematical model for describing the retinal nerve fiber bundle trajectories in the human eye: average course, variability, and influence of refraction, optic disc size and optic disc position. Exp Eye Res 2012;105:70-8.
38. Minckler DS. The organization of nerve fiber bundles in the Primate optic nerve head. Arch Ophthalmol 1980;98:1630-6.
39. Carreras FJ. Pathogenesis of glaucoma: how to prevent ganglion cell from axonal destruction? Neural Regen Res 2014;9:2046-7.
40. Carreras FJ, Porcel D, Guerra-Tschuschke I, et al. Fenestrations and preferential flow routes in the prelaminar optic nerve through wet scanning electron microscope and perfusion of tracers. Clin Experiment Ophthalmol 2010;38:705-17.
41. Frisen LA. Clinical test of vision. New York: Raven Press, 1990.
42. Bouhenni RA, Dunmire J, Sewell A, et al. Animal models of glaucoma. J Biomed Biotechnol 2012;2012:692609.
43. Nucci C, Osbornec NN, Bagetta G, et al. Glaucoma: an open-window to neurodegeneration and neuroprotection. Preface. Prog Brain Res 2008;173:xi.
44. Tariq YM, Li H, Burlutsky G, et al. Retinal nerve fiber layer and optic disc measurements by spectral domain OCT: normative values and associations in young adults. Eye (Lond) 2012;26:1563-70.
45. Cheung CYL, Leung CK. A Practical Guide for Interpretation of Optical Coherence Tomography Retinal Nerve Fiber Layer Measurement. J Curr Glaucoma Pract 2009;3:9-13.
46. Budenz DL, Anderson DR, Varma R, et al. Determinants of normal retinal nerve fiber layer thickness measured by Stratus OCT. Ophthalmology 2007;114:1046-52.
47. Aydin A, Wollstein G, Price LL, et al. Optical coherence tomography assessment of retinal nerve fiber layer thickness changes after glaucoma surgery. Ophthalmology 2003;110:1506-11.
48. Pollet-Villard F, Chiquet C, Romanet JP, et al. Structure-function relationships with spectral-domain optical

coherence tomography retinal nerve fiber layer and optic nerve head measurements. Invest Ophthalmol Vis Sci 2014;55:2953-62.

49. McDonnell JM. Ocular embryology and anatomy. In: Ryan SJ. editor. Retina. St. Louis: Mosby, 1989 .

doi: 10.21037/aes.2017.05.03

Cite this article as: Carreras FJ, Delgado ÁV, García-Serrano JL, Medina-Quero J. A virtual model of the retina based on histological data as a tool for evaluation of the visual fields. Ann Eye Sci 2017;2:28.